ELSEVIER

Biophysical Chemistry 71 (1998) 51–62

Biophysical Chemistry

A long-lifetime Ru(II) metal–ligand complex as a membrane probe

Xiang-Qun Guo [1], Felix N. Castellano, Li Li, Joseph R. Lakowicz *

Center for Fluorescence Spectroscopy, Department of Biochemistry and Molecular Biology and Medical Biotechnology Center, University of Maryland School of Medicine, 725 West Lombard Street, Baltimore, MD 21201, USA

Received 14 July 1997; revised 27 November 1997; accepted 27 November 1997

Abstract

A luminescent metal–ligand complex, $[Ru(bpy)_2(dppz)]^{2+}$, (where dppz is dipyrido[3,2-a:2′,3′-c] phenazine), was used as a photoluminescence probe for investigating submicrosecond lipid dynamics in a dipalmitoyl-L-α-phosphotidylglycerol (DPPG) model bilayer system. The luminescence of $[Ru(bpy)_2(dppz)]^{2+}$ in buffer is completely quenched but becomes luminescent when intercalated into DPPG vesicles. The experimental results show that the emission intensity of $[Ru(bpy)_2(dppz)]^{2+}$ intercalated into DPPG vesicles increases dramatically as temperature is increased towards the lipid phase transition temperature. This effect is abolished in bilayers containing a high concentration (>30 mol%) of cholesterol, suggesting this probe is sensitive to the membrane composition. Frequency-domain emission intensity decays, measured as a function of increasing temperature towards the lipid phase transition temperature (2 to 57°C), display two major lifetime components. The short lifetime disappears at temperatures well above the phase transition temperature. A comparison of oxygen quenching with iodide quenching suggests the heterogeneity of probe location at temperatures well below the lipid phase transition temperature and the homogeneity of probe location at temperatures well above the lipid phase transition temperature. $[Ru(bpy)_2(dppz)]^{2+}$ displays polarized emission, enabling the study of membrane dynamics. The long decay time displayed by this probe allows measurement of the overall rotational correlation time of lipid vesicles on the microsecond time-scale. Because of the long lifetime, polarized emission, and background free nature of the photoluminescence measurements, $[Ru(bpy)_2(dppz)]^{2+}$ has numerous applications in the biophysical studies of membranes. © 1998 Elsevier Science B.V.

Keywords: Metal–ligand complex; Photoluminescence; Fluorescence spectroscopy

1. Introduction

Fluorescence spectroscopy has been widely utilized in the study of the structure and dynamics of cell membranes [1–3]. Cell membranes are predominantly composed of phospholipids, which are spectroscopically silent in the ultraviolet and visible regions of the spectrum. Consequently, extrinsic fluorophores embedded in membranes or covalently attached to phospholipids are used in the study of membranes [4–7]. For instance, fluorescence probes have been used to monitor the conversion of phos-

* Corresponding author.

[1] On sabbatical leave from Department of Chemistry, Xiamen University, Xiamen, 361005, China.

PII S0301-4622(97)00135-X

pholipid bilayers from the lamellar to nonlamellar states [8], to study lipid packing fluctuations [9], and to measure membrane fusion [10]. Fluorescence spectroscopy has been used to study hydration in lipid bilayers [11]. The vast majority of traditional membrane probes, however, display decay times of 1–10 ns. As a result, dynamic fluorescence studies of lipid bilayers have been restricted to the nanosecond regimen, and most experiments are not able to reveal dynamic processes or phenomena in bilayers on the microsecond time-scale. The limitations of short decay times have been circumvented by using phosphorescence probes [12–14]. The use of phosphorescence, however, requires the complete exclusion of oxygen, and the phosphorescence time-zero anisotropies are often low.

More recently, metal–ligand probes with decay times from 0.5 to 1 μs have been used as biophysical probes. Importantly, ruthenium(II) (Ru), rhenium(I) (Re) and osmium(II) (Os) metal–ligand complexes display high anisotropy in the absence of rotational diffusion [15–18]. Metal–ligand complexes can display luminescence decay times ranging from <100 ns to 100 μs [19,20]. The observation of polarized emission combined with the long decay times available with these probes extends the observable time-scale of dynamic anisotropy measurements to ranges previously unavailable.

$[Ru(bpy)_2(dppz)]^{2+}$ has been used to probe the submicrosecond dynamics of DNA [15,39]. The results showed that $[Ru(bpy)_2(dppz)]^{2+}$ displays high anisotropy in vitrified solution, thus making it a useful anisotropy probe. The intensity and anisotropy decays of the DNA-bound probe extended past 450 ns. Time-resolved anisotropy measurements of proteins were extended to the microseconds time-scale using other metal–ligand complexes. Ru(II) metal–ligand complexes covalently linked to human serum albumin, concanavalin A, human immunoglobulin G and Ferritin demonstrated that this class of probes could be used to measure rotational correlation times as long as 1.5 μs [21], which so far has been inaccessible using routinely used fluorophores. Fluorescence polarization immunoassays in which metal–ligand complexes bound to human serum albumin demonstrated the potential of metal–ligand complexes in fluorescence polarization immunoassays of high-molecular-weight analytes [17]. When metal–ligand complexes were used as luminescence probes of lipid dynamics, the long decay times allowed measurement of the overall rotation correlation time of lipid vesicles to several microseconds [7]. Microsecond and submicrosecond dynamics of lipid bilayers has not been explored in any great depth. The need for additional long-lived membrane probes and the promising nature of metal–ligand complexes stimulated the present research.

Our experiments focus on the characterization of a luminescent ruthenium(II) metal–ligand complex, $[Ru(bpy)_2(dppz)]^{2+}$, (bpy = 2,2′-bipyridine, dppz = dipyrido[3,2-a:2′,3′-c] phenazine, Fig. 1), when used as a luminescence probe of lipid dynamics. Friedman et al. [22], Hartshorn and Barton [23] and Jenkins et al. [24] have pioneered the use of this particular metal–ligand compound to probe DNA structure. $[Ru(bpy)_2(dppz)]^{2+}$ displays no photoluminescence in aqueous solution at ambient temperature, but displays intense emission when intercalated into double-helical DNA and responds sensitively to subtle changes in the structure of the helix. These results were interpreted in terms of the shielding of the phenazine portion of the probe from the water molecules by intercalation of this highly planar ligand between the nucleotide bases. In the present research, we report that $[Ru(bpy)_2(dppz)]^{2+}$ can also be used as a lipid membrane probe. The results demonstrate that $[Ru(bpy)_2(dppz)]^{2+}$ is highly emis-

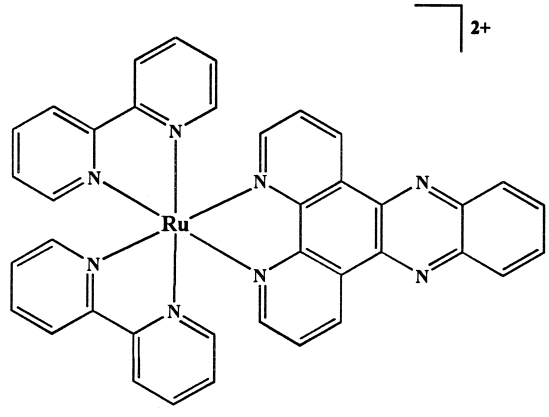

$[Ru(bpy)_2(dppz)]^{2+}$

Fig. 1. Molecular structure of *cis*-$[Ru(bpy)_2(dppz)]^{2+}$.

sive in phospholipid vesicles, although its luminescence in water is completely quenched. The sensitivity of the spectral properties of $[Ru(bpy)_2(dppz)]^{2+}$ to environment makes it possible to use this complex for probing lipid dynamics in model membranes.

2. Materials and methods

$[Ru(bpy)_2(dppz)](PF_6)_2$ was synthesized as described previously [15]. The purity of this compound was confirmed by NMR and elemental analysis. This complex exists only in the *cis*-form and is a mixture of two optical isomers (Λ- and Δ-) which display identical photophysical characteristics. The photoluminescence lifetime of this complex in dry, deaerated acetonitrile was 750 ns (single exponential) and was found to be nonemissive in water and in pH 7 buffer. All chemicals and solvents were reagent grade and used without further purification. Water was deionized with a Milli-Q system.

2.1. Preparation of lipid vesicles

Dipalmitoyl-L-α-phosphotidylglycerol (DPPG) was obtained from Sigma Chemical and used without further purification. For vesicle preparation, three different procedures were used.

2.1.1. Procedure 1

Lipids with a $[Ru(bpy)_2(dppz)]^{2+}$/DPPG mole ratio of 1:20 to 1:560 were suspended in a buffer solutions containing 10 mM Tris and 50 mM KCl, pH 7.5, at a final lipid concentration of 2.0 mM. Vesicles were prepared by sonicating the $[Ru(bpy)_2(dppz)]^{2+}$/DPPG solutions in a water bath at a constant temperature of 55°C, well above the phospholipid phase transition temperature (41°C). Removal of unincorporated $[Ru(bpy)_2(dppz)]^{2+}$ was achieved by passing the vesicle solution down a Sephadex G-25 column (10 cm × 1.2 cm), using Tris buffer as the eluent. The excluded fraction corresponding to the luminescent band was collected.

2.1.2. Procedure 2

Procedure 2 was basically the same as procedure 1 except it excluded the gel filtration step, since $[Ru(bpy)_2(dppz)]^{2+}$ did not display any luminescence when free in Tris buffer. If there was any free $[Ru(bpy)_2(dppz)]^{2+}$, it would not contribute to the luminescence intensity in the system. The experimental data from procedures 1 and 2 did not show significant variation in terms of luminescence intensity, anisotropy and lifetime.

2.1.3. Procedure 3

DPPG was suspended in Tris buffer, at a final concentration of 2.0 mM and vesicles were prepared by sonication in a water bath at 55°C. Vesicles were then labeled using $[Ru(bpy)_2(dppz)]^{2+}$ by direct solvent injection from a stock solution in Tris buffer, while keeping the DPPG vesicle solution in a water bath at constant temperature (55°C). Different $[Ru(bpy)_2(dppz)]^{2+}$/DPPG mole ratios were obtained by adding different amounts of $[Ru(bpy)_2(dppz)]^{2+}$ into the DPPG vesicle solution. Labelled vesicles were incubated at 55°C for 2 h to ensure complete uptake of $[Ru(bpy)_2(dppz)]^{2+}$. The experimental results obtained from procedure 3 did not show significant difference, when compared to that obtained from the other two procedures. In the case of anisotropy decay measurements, only procedure 2 was used to prepare the vesicle samples.

In all cases, vesicle samples with no $[Ru(bpy)_2(dppz)]^{2+}$ were prepared following procedure 3 and used to assess background vesicle scatter at the respective phospholipid concentrations, which was subsequently subtracted from the corresponding spectroscopic data. The background due to vesicles was typically less than 2% of the total signal intensity.

2.2. Instrumentation

Absorption spectra were recorded on a HP 8453 UV–Visible Spectrophotometer, and emission spectra were recorded on a SLM AB2 Spectrofluorimeter. The frequency-domain instrumentation (ISS) was used for all measurements of luminescence intensity and anisotropy decays. The excitation source was a CW air-cooled argon ion laser (543-AP, Omnichrome). The laser was amplitude modulated by an electro-optical low-frequency modulator and was tuned at 488.0 nm for excitation. In some cases, we measured high frequency intensity decays (to 150 MHz) with a PTS frequency synthesizer output into

a high frequency amplifier (ENI) which was used to drive the Pockels cell. In all measurements, a 610 nm cutoff filter (Corning 2-61) was used to isolate the emission of the Ru(II) samples. Texas Red in water was used as a lifetime reference sample.

Excitation anisotropy spectra were collected, with the anisotropy defined by:

$$r = \frac{I_{\parallel} - I_{\perp}}{I_{\parallel} + 2I_{\perp}} \quad (1)$$

where $I_{\parallel}$ and $I_{\perp}$ are the intensities measured with vertically polarized excitation and the emission polarization parallel ($I_{\parallel}$) or perpendicular ($I_{\perp}$) to the excitation. The values of the polarized intensities were corrected for the transmission efficiency of the polarized components by the detection optics. The excitation anisotropy spectrum of $[Ru(bpy)_2(dppz)]^{2+}$ embedded in DPPG vesicles was corrected for background vesicle scatter by

$$r = \frac{\left(I_{\parallel}^{S} - I_{\parallel}^{B}\right) - \left(I_{\perp}^{S} - I_{\perp}^{B}\right)}{\left(I_{\parallel}^{S} - I_{\parallel}^{B}\right) + 2\left(I_{\perp}^{S} - I_{\perp}^{B}\right)} \quad (2)$$

where the superscripts, S and B, denote the vesicle samples in the presence (S) and absence (B) of $[Ru(bpy)_2(dppz)]^{2+}$, respectively.

The frequency-domain intensity and anisotropy data were fitted by a nonlinear least squares procedure. The intensity decays were described by

$$I(t) = \sum_i \alpha_i e^{-t/\tau_i} \quad (3)$$

where $I(t)$ is the luminescence intensity at time t, and the α_i and the τ_i are the preexponential weighting factors and the excited-state lifetimes, respectively. The subscripts denote each component. Mean lifetimes were calculated using

$$\langle \tau \rangle = \sum_i \alpha_i \tau_i^2 / \sum_i \alpha_i \tau_i \quad (4)$$

Anisotropy decays were fit to a multi-exponential model:

$$r(t) = \sum_i r_{0i} e^{-t/\theta_i} \quad (5)$$

where r_{0i} are the amplitudes and θ_i are the correlation times of each component.

3. Results and discussion

3.1. Absorption spectra

Typical absorption spectra of $[Ru(bpy)_2(dppz)]^{2+}$ free in Tris buffer and in the presence of DPPG vesicles are shown in Fig. 2. The spectral maximum of the low-energy absorption band at 444 nm is the characteristic metal-to-ligand charge transfer (MLCT) transition. In the presence of DPPG model bilayers, significant spectral changes are observed with $[Ru(bpy)_2(dppz)]^{2+}$. The MLCT band increases significantly, whereas the π–π^* transition of the dppz ligand at $\sim$380 nm displays a hypochromic effect. These results are consistent with the behavior this complex displays upon binding to double helical DNA [38].

3.2. Steady state photoluminescence studies

$[Ru(bpy)_2(dppz)]^{2+}$ possesses an important luminescence characteristic. In aqueous solutions at ambient temperature the luminescence of the complex is completely quenched, yet it emits intensely when intercalated into DPPG vesicles, as shown in Fig. 3. We interpret this photoluminescence enhancement as a result of the anchorage of the planar dppz ligand to the membrane, effectively shielding it from water. Electrochemical and photophysical measurements of $[Ru(bpy)_2(dppz)]^{2+}$ in its ground and excited states

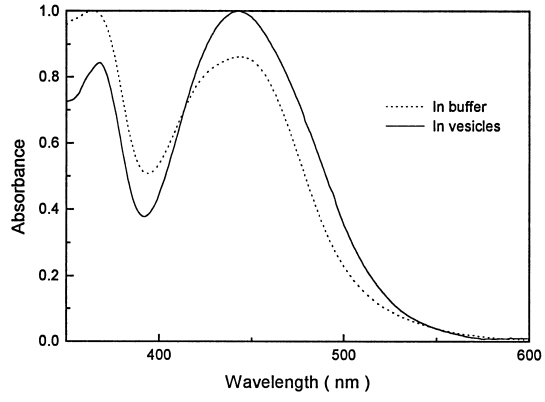

Fig. 2. Absorption spectra of $[Ru(bpy)_2(dppz)]^{2+}$ free and embedded in DPPG vesicles at 20°C, in pH 7.5 Tris buffer.

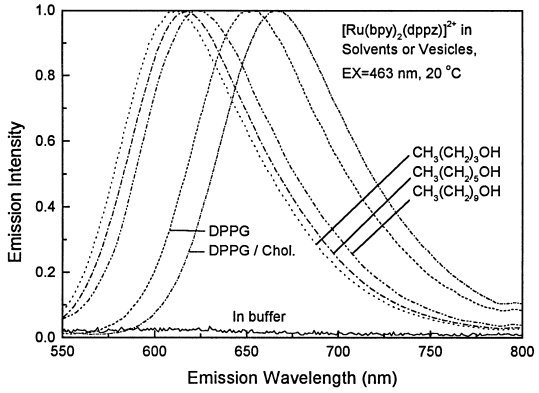

Fig. 3. Emission spectra of $[Ru(bpy)_2(dppz)]^{2+}$ free in several solvents: Tris buffer, 1-butanol, 1-hexanol, and 1-decanol. Also shown are the emission spectra with $[Ru(bpy)_2(dppz)]^{2+}$ embedded in DPPG vesicles composed of pure phospholipids and vesicles composed of phospholipids with cholesterol (50 mol%). Samples were excited at 463 nm with an excitation and emission bandpass of 8 nm at 20°C. These spectra are normalized to unity to facilitate comparison.

show that the charge transfer is directed from the metal center to the phenazine portion of the ligand, and the major nonradiative deactivation pathway for the complex likely involves the protonation of the phenazine nitrogen atoms in the excited state [25,26]. Therefore, embedding the probe in membranes protects the phenazine nitrogen atoms from interaction with water, thus decreasing the nonradiative deactivation quenching pathway.

For use of this metal–ligand complex as a lipid probe, the position where $[Ru(bpy)_2(dppz)]^{2+}$ localizes should be known. In order to explore this location, the emission properties of $[Ru(bpy)_2(dppz)]^{2+}$ in alcohols with linear alkyl chains of different lengths have been studied [27]. The wavelength maximum of emission intensity is approximately the same for methanol, ethanol, and 1-butanol. It shifts towards lower energies as the length of the alkyl chain is increased beyond 1-butanol, as shown in Fig. 3. The emission maximum shifts from 611 nm in 1-butanol to 624 nm in 1-decanol, a result in agreement with that previously reported [27]. Compared with emission in alcohols, the emission maximum in DPPG vesicles shifts towards still lower energy, 650 nm. Considering DPPG has a dipalmitoyl group, this result is consistent with an increase in the alkyl chain length. In fact, this steady state emission data correlates well with that found for $[Ru(bpy)_2(dppz)]^{2+}$ in micellar sodium dodecyl sulfate solutions [27]. These results suggest that the hydrophobic dipyridophenazine ligand of the complex is effectively buried in the bilayer, so that water molecules cannot interact with it and quench the emission of the complex.

Dynamic lipid packing fluctuations or phase transition within membranes are proposed to be responsible for many membrane-mediated events. We questioned whether $[Ru(bpy)_2(dppz)]^{2+}$ would be able to probe such dynamic events in lipid membranes. The emission intensities were measured as a function of increasing temperature towards the lipid phase transition temperature (T_c) (Fig. 4). The experiment showed a sharp increase of emission intensity at the transition temperature. We did not expect the emis-

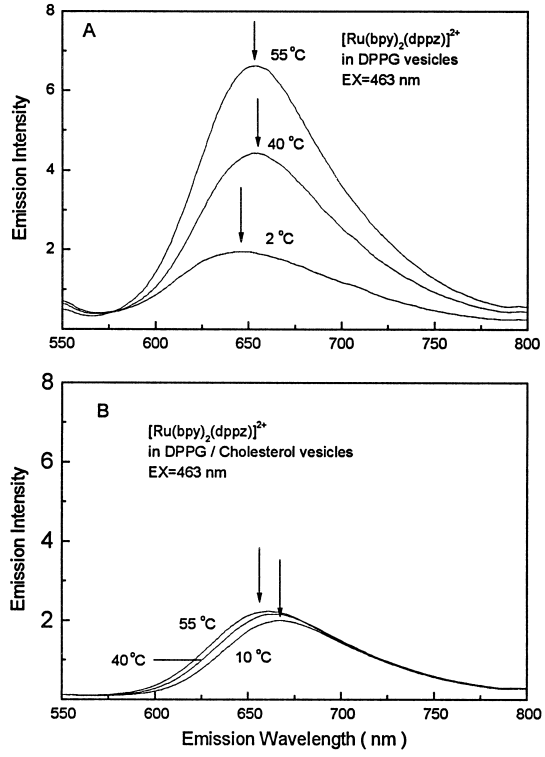

Fig. 4. Emission spectra of $[Ru(bpy)_2(bppz)]^{2+}$ embedded in DPPG vesicles (A) and DPPG vesicles composed of 50% mole cholesterol (B), measured as a function of increasing temperature towards the lipid phase transition temperature. Samples were excited at 463 nm with an excitation and emission bandpass of 8 nm.

sion intensity to increase as the temperature was increased. This behavior is quite peculiar since the emission intensity of most luminophores, especially Ru(II) MLCT complexes, decreases as the temperature is increased due to the enhancement of nonradiative decay pathways. The same results were obtained when the $[Ru(bpy)_2(dppz)]^{2+}$/DPPG mole ratio was changed from 1:70 to 1:560. We interpret these results in terms of $[Ru(bpy)_2(dppz)]^{2+}$ molecules being partially buried in bilayers at temperatures below the lipid phase transition temperatures, whereas the complex becomes more soluble (more shielded from H_2O) in the membrane at elevated temperatures. $[Ru(bpy)_2(dppz)]^{2+}$ carries two positive charges, whereas the head of DPPG carries one negative charge on the phosphate group. Based solely on electrostatic interactions, $[Ru(bpy)_2(dppz)]^{2+}$ is likely to localize at the lipid–water interface. The hydrophobic dipyridophenazine ligand, however, is likely to be trapped inside the bilayer. The competition between these two possible interactions depends on temperature. At low temperature, lipids pack in a more orderly form, that is a 'gel-like' form, where only a small fraction of $[Ru(bpy)_2(dppz)]^{2+}$ molecules are able to partition in the bilayer. At higher temperatures, above the lipid phase transition temperature, the membranes are less ordered, and $[Ru(bpy)_2(dppz)]^{2+}$ is more likely intercalated into the bilayer. This is evidenced by the increase in photoluminescence intensity with increasing temperature, which is a direct result of protection from water quenching. In fact, almost 100% of $[Ru(bpy)_2(dppz)]^{2+}$ molecules are buried in the interior region of the bilayer at temperatures above the phase transition temperature, as the intensity decay results show below.

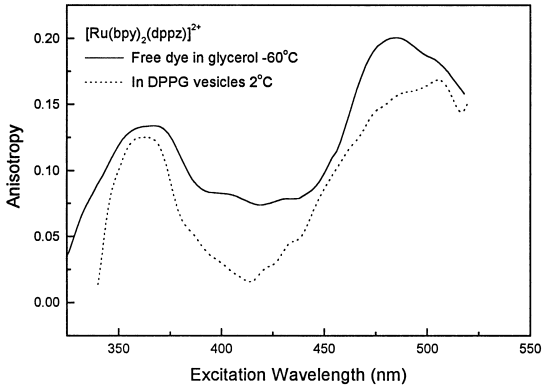

Fig. 6. Excitation anisotropy spectra of $[Ru(bpy)_2(dppz)]^{2+}$ free in glycerol at −60°C, and embedded in DPPG vesicles in Tris buffer, pH 7.5, at 2°C. Emission wavelength was 650 nm with an excitation and emission bandpass of 8 nm.

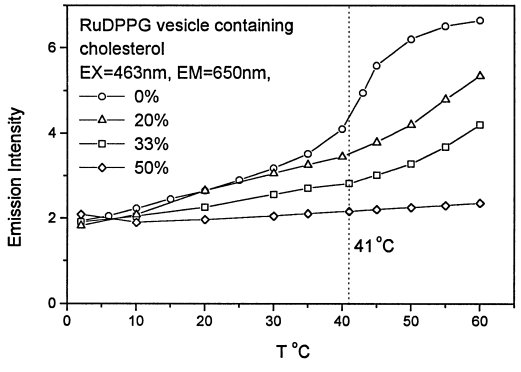

Fig. 5. Emission intensities of DPPG vesicles labeled with $[Ru(bpy)_2(dppz)]^{2+}$ at various cholesterol concentrations, measured as a function of increasing temperature towards the lipid phase transition temperature. Emission was measured at 650 nm (excited at 463 nm) with an excitation and emission bandpass of 8 nm.

Previous spectroscopic studies reported a strong modification of phase properties of phospholipids in the presence of cholesterol [28]. For $[Ru(bpy)_2(dppz)]^{2+}$, the emission maximum shifts to the longer wavelength upon addition of cholesterol (Fig. 3) and the degree of this shift is temperature dependent (Fig. 4). The increase in emission intensity at the phase transition temperature is smoothed by addition of cholesterol, as shown in Fig. 5. The lower photoluminescence intensity in the presence of cholesterol is a result of decreased membrane fluidity as its rigid steroid ring system interferes with the motions of the lipid side chains. It is therefore difficult for the probe to partition into the membrane in the presence of cholesterol. The red shift of the emission maximum in vesicles composed of binary mixtures of cholesterol and phospholipids is attributed to the more hydrophobic microenvironments than those in vesicles composed of pure phospholipids. These experimental results suggest that $[Ru(bpy)_2(dppz)]^{2+}$ is sensitive to lipid packing fluctuations and local hydration [29].

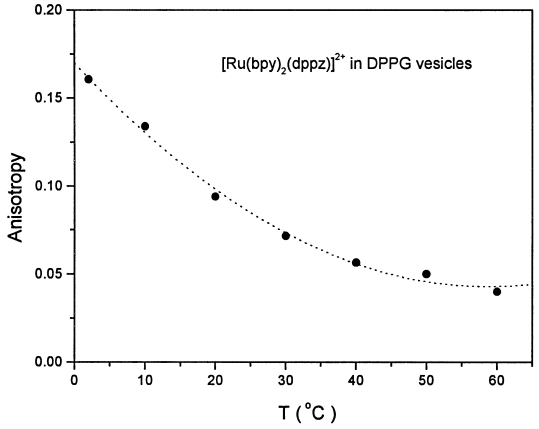

Fig. 7. Steady-state anisotropy of $[Ru(bpy)_2(dppz)]^{2+}$ embedded in DPPG vesicles with a molar ratio of $[Ru(bpy)_2(dppz)]^{2+}$/DPPG = 1:70, measured as a function of increasing temperature. The emission was monitored at 650 ± 4 nm, with 490 ± 4 nm excitation.

For use as a lipid hydrodynamic probe, $[Ru(bpy)_2(dppz)]^{2+}$ needs to display polarized emission. The excitation anisotropy spectra of $[Ru(bpy)_2(dppz)]^{2+}$ free in glycerol (-60°C) and partitioned into DPPG model vesicles (-2°C) are shown in Fig. 6. In the absence of rotational diffusion, $[Ru(bpy)_2(dppz)]^{2+}$ displays a maximum anisotropy of 0.14 at 360 nm and 0.20 at 480 nm. When intercalated into DPPG vesicles, it possesses a maximum anisotropy of 0.13 at 360 nm and 0.17 at 480–500 nm. These values are adequate for measurement of steady state and time-resolved anisotropy. We examined the steady state anisotropy of $[Ru(bpy)_2(dppz)]^{2+}$ buried in DPPG vesicles over a range of temperatures above and below the lipid phase transition temperature of 41°C. The anisotropy decreased progressively with increasing temperature as expected for thermally activated motions (Fig. 7). However, there was no sharp phase transition of the type seen with DPH-labelled membranes [30,31]. We attribute this to only a small fraction of $[Ru(bpy)_2(dppz)]^{2+}$ entering the interior region of the bilayer, while a large fraction of $[Ru(bpy)_2(dppz)]^{2+}$ localizes near the lipid–water surface at temperatures below the lipid phase transition. Above the phase transition, there still is adequate anisotropy for measurement, unlike the previously reported $[Ru(bpy)_2(mcbpy)]^{2+}$ labeled lipid probe, which was totally localized at the lipid–water surface and its anisotropy decreased towards zero at temperatures above the phase transition temperature [7]. These results are in agreement with the hypothesis that $[Ru(bpy)_2(dppz)]^{2+}$ molecules are almost totally buried in the interior region of the bilayer at temperatures above the phase transition temperature.

3.3. Time-resolved photoluminescence intensity decay studies

Frequency-domain intensity decays of DPPG vesicles labeled with $[Ru(bpy)_2(dppz)]^{2+}$ were measured over a range of temperatures spanning the phase transition temperature. It should be noted that this complex displays a single exponential lifetime in aprotic solvents like CH_3CN (750 ns) [15,39]. Typical frequency-domain intensity decays are shown in Fig. 8. Multi-exponential analysis of the frequency-domain intensity decays are summarized in Table 1. The decays at temperatures below the phase transition were best fit using a sum of three exponential components. We believe that the shortest component near 8 ns is due to scattered light. The major decay components include a long decay time τ_1 and an intermediate decay lifetime τ_2. The longer lifetime is sensitive to temperature, resulting in lifetime quenching from 290 ns to 125 ns, corresponding to an increase in temperature from 2 to 57°C. In contrast, the intermediate lifetime is temperature invariant, as

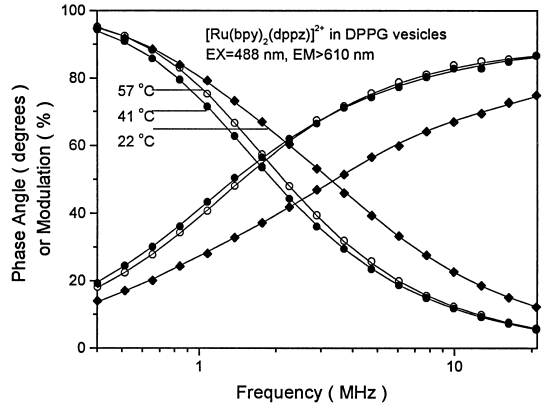

Fig. 8. Frequency-domain intensity decays of $[Ru(bpy)_2(dppz)]^{2+}$ embedded in DPPG vesicles at various temperatures.

Table 1
Summary of the frequency-domain intensity decays of $[Ru(bpy)_2(dppz)]^{2+}$ embedded in DPPG vesicles

[Ru]: [DPPG] (mole ratio)	T (°C)	τ_i (ns)	α_i	Mean τ (ns)	χ_R^2 (χ_R^2)[a]
1:70	2	293.2	0.128		
		52.9	0.321		
		6.2	0.550	205.8	1.85 (742.45)
	10	260.0	0.128		
		51.2	0.424		
		7.2	0.440	168.3	1.81 (459.19)
	22	199.8	0.138		
		49.8	0.580		0.78 (178.20)
		10.0	0.282	117.5	
	27	167.2	0.148		
		49.0	0.560		1.13 (149.65)
		8.4	0.292	101.9	
	32	182.3	0.152		
		70.4	0.484		1.85 (78.45)
		22.9	0.360	98.6	
	41	146.2	0.885		0.87 (4.3)
		42.5	0.115	142.4	
	48	136.9	0.760		1.78 (7.49)
		66.0	0.236	128.0	
					0.66 (0.66)
	55	128.7	1	128.7	
					1.63 (1.63)
	57	125.6	1	125.6	
1:560	3	284.3	0.05		
		51.3	0.30		
		12.1	0.64	150.0	1.87 (721.09)
	25	188.0	0.06		
		51.2	0.63		
		12.1	0.325	81.2	0.87 (159.63)
	36	202.2	0.05		
		79.2	0.42		1.43 (93.65)
		27.5	0.53	95.8	
					1.80 (1.80)
	51	139.6	1	139.6	

[a] Number in parenthesis is χ_R^2 recovered from a fit to a single-exponential decay law.

shown in Fig. 9. It is interesting to note that the decays at temperatures above the phase transition are closely approximated by single exponential decays, and the decay times are in linear correlation with the longer lifetimes obtained at lower temperatures. Multi-component lifetime decays of fluorescent dyes embedded in lipid vesicles have previously been observed for other, well known fluorescence membrane probes, such as DPH [30,31], perylene [32], and coronene [5]. In the case of DPH, the physical origins of the differences in lifetime value could be the result of a *cis-trans* photo-isomerization [33] or the relative orientation of the DPH molecule with respect to the membrane surface [34,35], or local value of the static dielectric constant [36]. We attribute the multi-component lifetime decays of $[Ru(bpy)_2(dppz)]^{2+}$ at temperatures below or near the phase transition to the heterogeneity of probe location, namely in the interior region of the bilayer or exposed to the lipid–water surface. This hypothesis is further confirmed by the fact that the fraction of the longer lifetime component, α_1, proves to be temperature variant. As shown in Fig. 10, α_1 increases rapidly near the phase transition temperature, and approaches unity at temperatures well above the phase transition. These results suggest that the probe

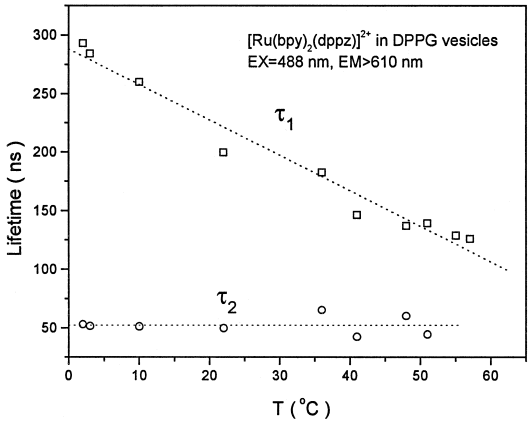

Fig. 9. Recovered emission lifetimes of $[Ru(bpy)_2(dppz)]^{2+}$ embedded in DPPG vesicles measured as a function of increasing towards the lipid phase transition temperature.

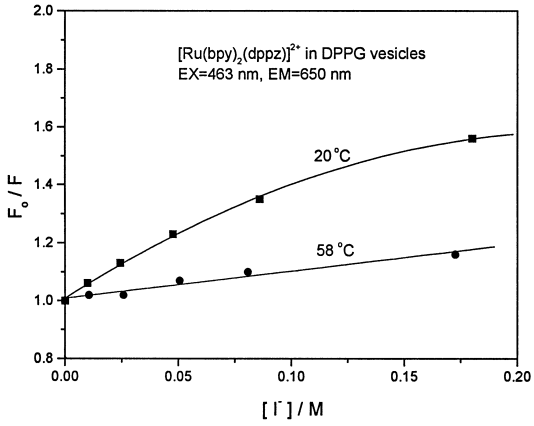

Fig. 11. Sterm–Volmer plot of iodide quenching of the emission of $[Ru(bpy)_2(dppz)]^{2+}$ embedded in DPPG vesicles, measured at 650 ± 4 nm excited at 463 ± 4 nm with excited at 463 ± 4 nm.

location is somewhat homogeneous at temperatures well above the phase transition temperature.

To further clarify the nature of the multi-component decays, a comparison of oxygen quenching to iodide quenching was made. In the case of iodide quenching, Stern–Volmer behavior was observed at temperatures below the lipid phase transition temperature (Fig. 11). At these temperatures, in contrast, frequency-domain intensity decays give more information than steady-state experimental data (Fig. 12). In the case of the intermediate lifetime component, addition of iodide ions results in a decrease in lifetime from 50 ns to 35 ns, at room temperature, corresponding to an increase in concentration of iodide from 0 to 0.16 M. The Stern–Volmer plot is approximately linear. The longer lifetime, however, appears to be invariant over the same range of iodide concentration. These results demonstrate that some of $[Ru(bpy)_2(dppz)]^{2+}$ molecules localize at interior region of lipid bilayer, and hence, are inaccessible to quenchers in the external aqueous phase. In addition, iodide quenching is less significant at temperatures above the lipid phase transition temperature (Fig.

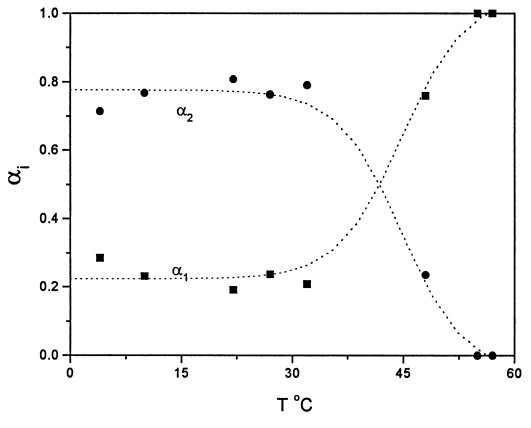

Fig. 10. Frequency-domain amplitude decay parameters, α_i, for DPPG vesicles labeled with $[Ru(bpy)_2(dppz)]^{2+}$, measured as a function of temperature ($\alpha_1 + \alpha_2 = 1$).

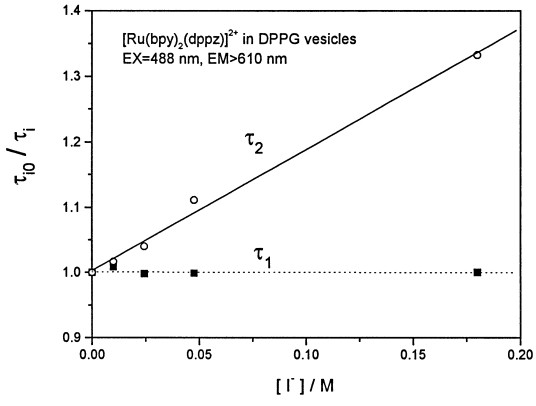

Fig. 12. Sterm–Volmer plot for iodine quenching of the frequency-domain intensity decay lifetimes of $[Ru(bpy)_2(dppz)]^{2+}$ embedded in DPPG vesicles, measured at room temperature. The unquenched decay times were $\tau_1 = 190$ ns, and $\tau_2 = 50$ ns.

11), suggesting that $[Ru(bpy)_2(dppz)]^{2+}$ molecules are shielded from the quencher in the aqueous phase. In the case of oxygen quenching, the longer lifetime component was found to be more sensitive to oxygen quenching than the intermediate lifetime component. The longer lifetime component is 136 ns in an oxygen equilibrated solution at room temperature as compared to 190 ns in the air-equilibrated solution. The intermediate lifetime component is 45 ns in oxygen-equilibrated solution which is only 10% quenched compared to 50 ns in an air-equilibrated solution. Fluctuations of the lipid molecules permit diffusion of oxygen into and within the interior region, and thus results in dynamic quenching of both components. A similar phenomenon has been previously observed by comparison of oxygen and iodide quenching of the tryptophan fluorescence in proteins [35,37].

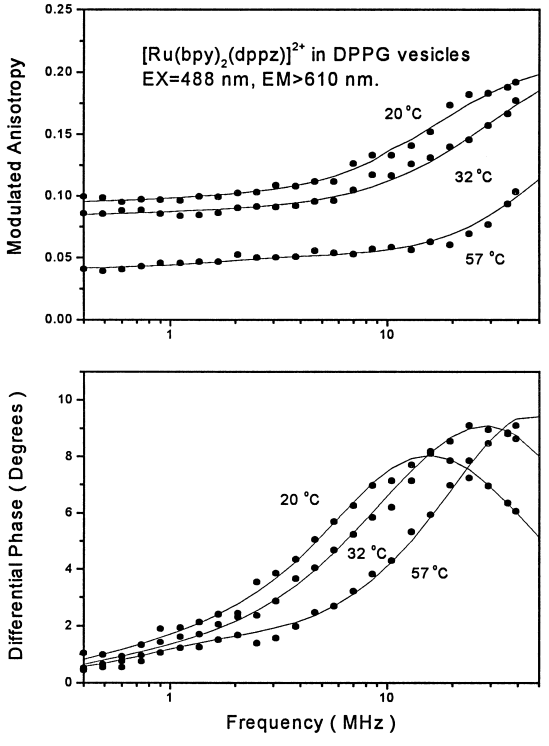

Fig. 13. Frequency-domain anisotropy decays of $[Ru(bpy)_2(dppz)]^{2+}$ embedded in DPPG vesicles measured as a function of temperature.

Table 2
Anisotropy decay analysis of $[Ru(bpy)_2(dppz)]^{2+}$ embedded in DPPG vesicles

T (°C)	θ_i (ns)	r_i	Σr_i^a	χ_R^2
2	>15000	0.0754		
	11.0	0.125	0.200	9.2
22	7342	0.0775		
	10.8	0.134	0.212	1.60
32	2386	0.0738		
	6.1	0.145	0.219	1.87
41	353	0.0561		
	6.1	0.124	0.181	2.07
47	225	0.0482		
	3.8	0.144	0.192	1.94
57	178	0.0547		
	3.6	0.110	0.165	2.3

[a]The measured anisotropy in the absence of rotational diffusion for 488 nm excitation is 0.2.

3.4. Time-resolved anisotropy decay studies

To evaluate the usefulness of $[Ru(bpy)_2(dppz)]^{2+}$ for studies of microsecond membrane dynamics, we examined the frequency-domain anisotropy decays of $[Ru(bpy)_2(dppz)]^{2+}$ in DPPG vesicles. Typical results are shown in Fig. 13. Analysis of these data in terms of a two-exponential anisotropy decay are summarized in Table 2. For all temperatures examined, both short and long correlation times are recovered, which are assigned to local probe motion and overall rotational diffusion of the phospholipid vesicle, respectively. At temperatures well below the lipid phase transition temperature, the lipid is presumed to be predominantly gel-like. Under such conditions, $[Ru(bpy)_2(dppz)]^{2+}$ is embedded in the bilayer and is partially immobilized. The longer correlation times are consistent with that expected for overall rotational diffusion of phospholipids vesicles with diameters from 300 to 500 A (Table 3). With

Table 3
Calculated rotational correlation times for membrane vesicles of various diameters[a]

Diameter (A)	200	250	300	400	500	600
θ (ns)	1034	2020	3490	8272	16156	27918

[a]Rotational correlation times (θ) were calculated from the Stokes Einstein equation $\theta = \eta V/RT$, where $\eta = 1$ cP is the viscosity, $T = 297$ K, and V is the volume.

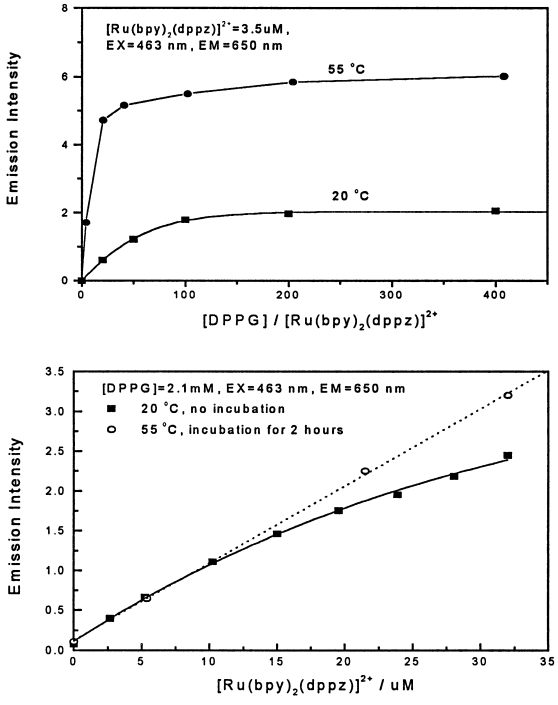

Fig. 14. Influence of the molar ratio of DPPG/$[Ru(bpy)_2(dppz)]^{2+}$ on the emission intensity of $[Ru(bpy)_2(dppz)]^{2+}$ embedded in DPPG vesicles. Top: measured indicated temperatures. Bottom: at 20°C with and without incubation for 2 h at 55°C.

increasing temperature, the amplitude of the longer correlation time decreases, consistent with an increased free probe motion. The longer correlation time becomes much shorter above the phase transition temperature, suggesting that the phase fluctuation-induced motion of the probe is more fluid-like. It is probable that this correlation time represents an average of the overall vesicle rotation. The fractional amplitude of the short correlation time remains relatively constant with temperature, suggesting that local probe motions contribute to the anisotropy decay at all temperatures.

Another important characteristic of this lipid probe is the extent of labelling possible without spectral changes resulting from probe–probe interactions. We examined the influence of different $[Ru(bpy)_2(dppz)]^{2+}$/DPPG ratios on the emission spectra, intensity decays, and quantum yields over a range of $[Ru(bpy)_2(dppz)]^{2+}$/DPPG mole ratios from 1:20 to 1:560. There were no significant differences except the emission intensities are lower when the ratio of DPPG/$[Ru(bpy)_2(dppz)]^{2+}$ is below 20 (Fig. 14). This absence of probe–probe interaction is consistent with the large Stokes' shift of the emission seen in Figs. 2 and 3.

4. Conclusions

$[Ru(bpy)_2(dppz)]^{2+}$, a nonluminescent metal–ligand complex in water, emits intensely when partitioned into DPPG model bilayers in aqueous solution and responds sensitively to the lipid phase transition, and subtle changes in the lipid microenvironment. These results demonstrate the use of this probe in investigating lipid packing fluctuations and local hydration. Its polarized emission was used in studies of membrane dynamics. The long intensity decay times allow for measurement of the overall rotational correlation time of lipid vesicles on a microsecond time-scale.

The results described in this report are for a quite novel intercalative lipid probe. Metal–ligand complexes, a versatile class of probes in terms of polarized emission, lifetimes, absorption and emission maxima, can offer numerous new experimental opportunities for the studies of membranes and other biomolecules.

Acknowledgements

This work was supported by a grant from the National Institutes of Health, (RR-08119), with support for instrumentation from the NIH (RR-07510-01). FNC is supported by the NIH with a postdoctoral fellowship (1F32-GM-18653). This work was also supported by the National Natural Science Foundation of China. XQG also expresses appreciation for support from the Department of Chemistry at Xiamen University, China.

References

[1] C.D. Stubbs, B.W. Williams, Topics in Fluorescence Spectroscopy, Biochemical Applications, vol. 3, in: J.R. Lakowicz, (Ed.), Plenum, New York, 1992, pp. 231–271.
[2] J.G. Dewey, (Ed.), Biophysical and Biochemical Aspects of

Fluorescence Spectroscopy, Plenum, New York, 1991, p. 294.
[3] L. Davenport, J.R. Knutson, L. Brand, Subcellular Biochemistry, in: J.R. Harris, A.H. Etemadi, (Eds.), Plenum, New York, 1989, pp. 145–188.
[4] J. Slavik, (Ed.), Fluorescence Probes in Cellular and Molecular Biology, CRC Press, Boca Raton, FL, 1994.
[5] L. Davenport, P. Targowski, Biophys. J. 71 (1996) 1837–1852.
[6] L. Li, H. Szmacinski, J.R. Lakowicz, Biospectroscopy 3 (1996) 155–159.
[7] L. Li, H. Szmacinski, J.R. Lakowicz, Anal. Biochem. 244 (1) (1997) 80–85.
[8] R.M. Epand, J. Fluorescence 5 (1) (1995) 1–8.
[9] L. Davenport, P. Targowski, J. Fluorescence 5 (1) (1995) 8–18.
[10] B.R. Lentz, J. Fluorescence 5 (1) (1995) 29–38.
[11] C.D. Stubbs, C. Ho, S.J. Slater, J. Fluorescence 5 (1) (1995) 19–28.
[12] A. Burkli, R.J. Cherry, Biochemistry 20 (1981) 138–145.
[13] J. Gonzalez-Rodriguez, A.U. Acuna, M.V. Alvarez, T.M. Jovin, Biochemistry 33 (1994) 266–274.
[14] J.C. Voss, J.E. Mahaney, L.R. Jones, D.D. Thomas, Biophys. J. 68 (1995) 1785–1795.
[15] J.R. Lakowicz, H. Malak, I. Gryczynski, F.N. Castellano, G.J. Meyer, Biospectroscopy 1 (1995) 163–168.
[16] J.R. Lakowicz, Z. Murtaza, W.E. Jones Jr., K. Kim, H. Szmacinski, J. Fluorescence 6 (1996) 245–249.
[17] E. Terpetshnig, H. Szmacinski, J.R. Lakowicz, Anal. Biochemistry 227 (1995) 140–147.
[18] Z. Murtaza, L. Li, F.N. Castellano, H. Szmacinski, J.R. Lakowicz, Biophys. J. 71 (1997) Part 2. of 2, A201.
[19] G.A. Reitz, J.N. Demas, B.A. DeGraff, E.M. Stephens, J. Am. Chem. Soc. 110 (1988) 5051–5059.
[20] L. Sacksteder, M. Lee, J.N. Demas, B.A. DeGraff, J. Am. Chem. Soc. 115 (1993) 8230–8231.
[21] E. Terpetsching, H. Szmacinski, H. Malak, J.R. Lakowicz, Biophys. J. 68 (1995) 342–350.
[22] A.E. Friedman, J.-C. Chambron, J.-P. Sauvage, N.J. Turro, J.K. Barton, J. Am. Chem. Soc. 112 (1990) 4960–4962.
[23] R.M. Hartshorn, J.K. Barton, J. Am. Chem. Soc. 114 (1992) 5919–5925.
[24] Y. Jenkins, A.E. Fridman, N.J. Turro, J.K. Barton, Biochemistry 31 (1992) 10809–10816.
[25] J.-C. Charmbron, J.-P. Sauvage, E. Amouyal, P. Koffi, New J. Chem. 9 (1985) 527–529.
[26] E. Amouyal, A. Homsl, J.-C. Charmbron, J.-P. Sauvage, J. Chem. Soc., Dalton Trans., 1990, pp. 1841–1845.
[27] J.-C. Charmbron, J.-P. Sauvage, Chem. Phys. Lett. 182 (6) (1991) 603–607.
[28] T. Parasassi, E. Gratton, J. Fluorescence 5 (1) (1995) 59–69.
[29] D. Voet, J.G. Voet, Biochemistry, Wiley, New York, 1990, p. 284.
[30] L.A. Chen, R.E. Dale, S. Roth, L. Brand, J. Biol. Chem. 252 (1977) 2163–2169.
[31] L. Davenport, R.E. Dale, R.H. Bisby, R.B. Cundall, Biochemistry 24 (1985) 4097–4108.
[32] J.R. Lakowicz, J.R. Knutson, Biochemistry 19 (1980) 905–911.
[33] K. Lunde, L. Zechmeister, J. Am. Chem. Soc. 76 (1954) 2308–2313.
[34] S. Wang, J.M. Beechem, E. Gratton, M. Glaser, Biochemistry 30 (1991) 5565–5572.
[35] D. Toptygin, L. Brand, J. Fluorescence 5 (1) (1995) 39–50.
[36] E. Gratton, T. Parasassi, J. Fluorescence 5 (1) (1995) 51–57.
[37] J.R. Lakowicz, Principles of Fluorescence Spectroscopy, Plenum, New York, 1983, pp. 278–279.
[38] C. Hiort, P. Lincoln, B. Norden, J. Am. Chem. Soc. 115 (1993) 3448–3454.
[39] H. Malak, I. Grycrynski, J.R. Lakowicz, G.J. Meyer, F.N. Castellano, J. Fluorescence 7 (2) (1997) 107–112.